BMC Complementary Medicine and Therapies

RESEARCH

Open Access

Flavonoids of *Andrographis paniculata* regulate hepatitis B virus replication and hepatocellular carcinoma progression: evidence from computational and experimental studies

Vishal S. Patil[1,2], Darasaguppe R. Harish[1*], Rajitha Charla[1], Vishwambhar Vishnu Bhandare[1], Swarup S. Gujarathi[1], Faizan A. Beerwala[1,2], Priyanka P. Patil[1,2], Sunil S. Jalalpure[1*], Harsha V. Hegde[1] and Subarna Roy[1]

Abstract

Background The HBx protein of hepatitis B virus (HBV) plays a crucial role in HBV pathogenesis, yet current treatments like HIV reverse transcriptase (RT) inhibitors, which target HBV RT due to similar active sites, have severe side effects, risk of drug resistance, and high costs. The present study investigates the anti-hepatitis B virus (HBV) properties of *Andrographis paniculata* (AP) and *Thespesia populnea* (TP) on HBV expressing HepG2.2.15 cells and by computational analysis.

Methods In vitro cytotoxicity, reverse transcriptase inhibitory, DNA and pgRNA quantification by qRT-PCR, time course analysis of HBsAg and HBeAg, and HBX-HBXIP interaction inhibition studies were conducted. The interaction of HBX with HBXIP, and phytocompounds' interaction with HBx was analyzed through molecular docking and dynamics studies.

Results AP exhibits lower cytotoxicity (CC_{50} = 832.915 µg/mL) than TP (CC_{50} = 593.122 µg/mL) after 24 h, with Tenofovir disoproxil fumarate (TDF) showing minimal cytotoxicity (CC_{50} > 500 µM). Both AP and TP significantly decreased intracellular HBV DNA with a > 2^5 fold reduction at higher concentrations (125–500 µg/mL) but had no significant effect on pgRNA level. AP and TP 500 µg/mL effectively inhibited HBsAg secretion (95% and 80% inhibition, respectively), over 120 h. AP also showed inhibition of HBeAg secretion (75–82%), while TP exhibited a higher inhibition of 90% at 24 h. TDF showed consistent but lower inhibitory effects on HBsAg and HBeAg. The HBx-HBXIP interaction inhibition assay showed AP's greater inhibitory capacity (IC_{50} < 62.5 µg/mL) compared to TP (IC_{50} = 806.69 µg/mL). Computational studies further validated these findings, showing stable binding interactions of AP compounds (flavonoids) with HBx protein (with Arg138 and His139, Lys140, and Trp141 residues participating

*Correspondence:
Darasaguppe R. Harish
harish.dr@icmr.gov.in
Sunil S. Jalalpure
jalalpuresunil@rediffmail.com

Full list of author information is available at the end of the article

in the interaction with HBXIP), corroborating their potential in disrupting HBV replication. Molecular dynamics simulations confirmed the stability of these interactions over 100ns.

Conclusions AP exhibits potent anti-HBV activities, making it a promising candidate for further therapeutic development.

Keywords *Andrographis paniculata*, Hepatitis B virus, HBx, HepG2.2.15, *In silico*

Background

Hepatitis B virus (HBV) is a DNA containing virus belonging to the family of *Hepadnaviridae*, that replicates in the liver cells of humans and other higher primates, causing hepatocellular carcinoma (HCC) and liver damage [1, 2]. The HBV virion contains a tiny, partially double-stranded, 3.2 kb relaxed circular DNA (rcDNA) genome. This genome converts into covalently closed circular DNA (cccDNA) and is translated to produce four different transcripts: pgRNA (3.5 kb), PreS1 (2.4 kb), PreS2 (2.1 kb), and X (0.7 kb). These transcripts produce polymerase, HBcAg, HBeAg, HBsAg, and HBx; have specific roles in the HBV life cycle [3, 4]. In 2022, the World Health Organization (WHO) projected that there were 254 million individuals living with chronic hepatitis B, with 65% of these people residing in the African and Western Pacific areas. HBV-related deaths rank tenth highest cause of death globally, with about 820,000 deaths worldwide reported each year [5, 6].

Sodium taurocholate cotransporting polypeptide (NTCP) is a key host receptor for the HBV to get into the cell [7]. Inside the hepatocytes, the relaxed circular DNA (rcDNA) transforms into a covalently closed circular DNA (cccDNA) that serves as the transcriptional template for the transcription of major viral mRNA [2]. Among the HBV proteins, the HBx is the smallest ORF coding 154-amino acid regulatory protein and is present in all Orthohepadnaviruses, or mammalian Hepadnaviruses [8]. The HBV-encoded oncogene X protein (HBx) is a crucial multifunctional regulatory protein that promotes viral replication and disrupts many cellular signaling pathways involved in virus-induced liver cancer development [9]. HBx regulates multiple signalling pathways including nuclear factor kappa-light-chain-enhancer of activated B cells (NF-kB), Janus kinase-signal transducer and activator of transcription (JAK-STAT), mitogen-activated protein kinase (MAPK), etc. Additionally, HBx has been linked to the control of apoptosis, calcium signalling, DNA repair, and cell cycle regulation [9].

For the management of HBV infection, WHO has approved several anti-viral medications these include interferons and nucleotide analogues (NA) like interferon alfa, pegylated interferon alfa-2a, lamivudine, adefovir, entecavir, telbivudine and tenofovir [10]. NA produces their action by inhibiting the reverse transcription enzyme which is required for HBV polymerization [11]. Although the NA and interferons are considered as the first-line treatment for HBV infection, have certain limitations. Flu-like symptoms, marrow suppression, anxiety, and depression, as well as autoimmune illnesses, including autoimmune thyroiditis, are adverse effects of pegylated interferon; strict medical supervision and laboratory testing are necessary. Although the majority of oral medications have tolerable side effects even after prolonged usage, frequent renal function monitoring is advised throughout nucleotide therapy because adefovir and tenofovir may have nephrotoxic consequences [12, 13]. Patients treated with telbivudine showed a higher occurrence of grade 3 and 4 increases in creatine kinase levels compared to those treated with lamivudine after 2 years of treatment. Telbivudine has also been associated with peripheral neuropathy. However, it also appears to have few significant toxic side effects [14, 15]. Hence it is necessary to find a novel bioactive with reduced adverse effects, better efficacy, and easy availability.

Plants have been a source of medicine for humans since ages. Due to its higher efficacy and lower adverse effects, traditional medicine has considerable attention for the treatment of several chronic infections and diseases [16]. Secondary metabolites or phytocompounds present in the plants are responsible for the pharmacological action produced by the plants. In our previous study, 11 phytocompounds from *Andrographis paniculata* (AP) and 3 from *Thespesia populnea* (TP) were predicted to regulate the host targets and pathways involved in the HBV pathogenesis [17]. The current investigation is further extended to study the effect of hydroalcoholic extract of AP and TP on HBV HBsAg, HBeAg, pgRNA, DNA levels, and HBx-HBXIP interactions. Figure 1 represents the brief outline of the outcome.

Materials and methods

Collection of plant materials and authentication

The whole plant of *Andrographis paniculata* burm.F. (AP) and the aerial part (Leaf and flower buds) of *Thespesia populnea* (L.) Sol. Ex Correa (TP) were picked from the local areas of Belagavi, Karnataka, India at the geographic coordinates 15°50'28.1"N 74°31'21.5"E and 15°52'54.9"N 74°31'29.2"E respectively. These plant parts were authenticated by a qualified plant taxonomist at Shri B.M.K Ayurveda Mahavidyalaya by Dr. Divya Khare, Department of Dravyaguna Vigyana and at ICMR- National

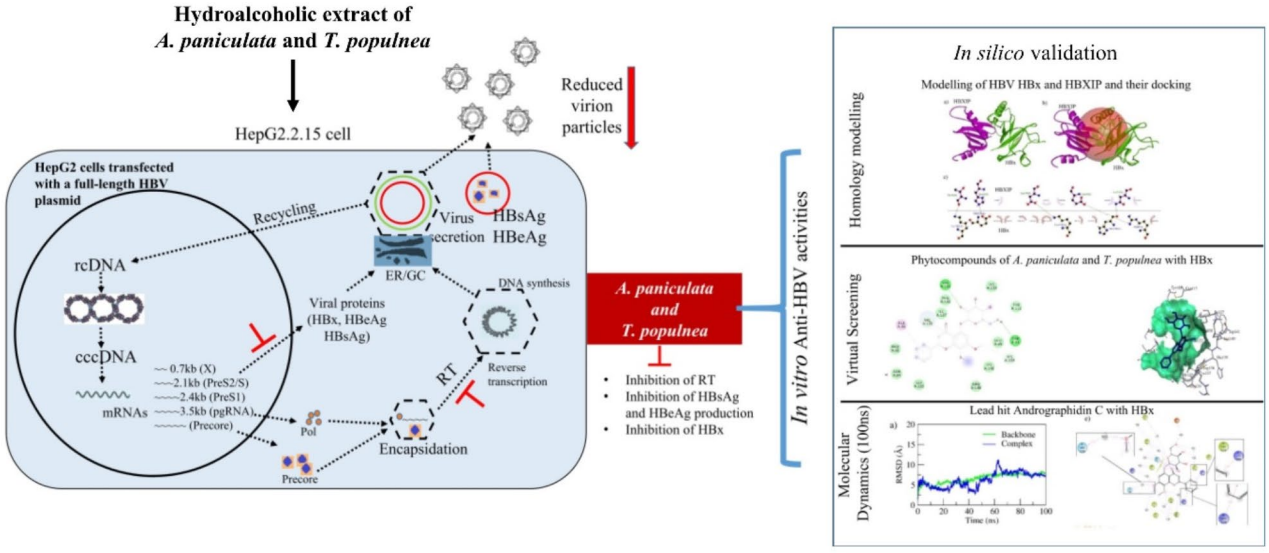

Fig. 1 Represents the in vitro and in silico studies workflow and the effect of AP and TP on the HBV life cycle and inhibition of HBx-HBXIP interaction

Institute of Traditional Medicine, Belagavi by Dr. Harsha V. Hegde, Scientist E, Department of Ethnomedicine, and the voucher specimens with assigned the accession numbers CFR/Auth/06/2023 and RMRC-1714 for AP and TP, respectively were deposited for future reference.

In vitro studies

Procurement and maintenance of HepG2.2.15 cell line

The HepG2.2.15 cell line is a derivative of the HepG2 human liver cancer cell line that maintains stable expression of the hepatitis B virus (HBV). The cell line was acquired from the International Centre for Genetic Engineering and Biotechnology (ICGEB) after obtaining the approvals from the Institutional Biosafety Committee (IBSC) (IBKP TAI No. C100753). The cells were maintained in Dulbecco's Modified Eagle's Medium (DMEM) enriched with 10% fetal bovine serum (FBS) and appropriate antibiotics (G418). The cells were subcultured and maintained until they achieved about 70% confluence in T25 flasks at a temperature of 37 °C with 5% carbon dioxide within a humidified incubator.

Preparation of test samples

The sample's stock concentration of 10 mg/mL in a solution of 5% DMSO in sterile water was prepared and was then filtered using a 0.22 µM syringe filter. Various quantities, ranging from 15.65 to 2000 µg/mL, were produced in DMEM from the available stock and used for further investigations.

MTT assay in HepG2.2.15 cell line

A total of 20,000 cells were seeded evenly into each well of 96-well flat-bottom plates and incubated for 24 h. Subsequently, the cells were exposed to various concentrations of the samples. The total volume in each well was adjusted to 250µL using DMEM medium with 2% FBS. The cells were then incubated for 24 h at a temperature of 37 °C with 5% CO_2. The next day, the wells were treated with 20 µL of MTT reagent (5 mg/mL concentration) and were then incubated for 4 h at a temperature of 37 °C with 5% CO_2. Following incubation, the supernatant was removed and wells were treated with 100 µL of 99.5% DMSO by gentle agitation to dissolve the formazan crystals. The absorbance was measured at 570 nm using a UV-Vis spectrophotometer. The cytotoxic activity was expressed as the percentage of viable cells, and the CC_{50} values were calculated using a linear regression curve [18].

$$\%\ Cell\ viability = \frac{\text{Abs of control} - \text{Abs of sample}}{\text{Abs of control}} \times 100$$

Time-course analysis of HBsAg and HBeAg

The cells were subjected to various concentrations of extracts/pure compounds. The level of HBsAg was assessed at time points of 24, 48, 72, 96, and 120 h, while HBeAg was assessed at time points of 24, 72, and 120 h in the culture medium. The HBsAg Hepalisa kit (purchased from J. Mitra & Co. Pvt. Ltd, Cat No. IR020096) for HBsAg measurement and the HBeAg Kit (purchased from Bioneovan Co. Ltd, Cat No. BE103A) for HBeAg measurement was used. The assay was carried out following the instructions provided by the manufacturers. The full procedure is provided in Supplementary Document 1. The calculation of the % inhibition of HBsAg and HBeAg is performed as follows,

$$\%\ Inhibition = \frac{Abs\ of\ control\ -\ Abs\ of\ sample}{Abs\ of\ control} \times 100$$

HBx-HBXIP interaction inhibition assay

The HBx-HBxIP interaction inhibition test was developed and standardized using HBxAg (KinesisDX, Cat No. K12-1594) and HBXIP (KinesisDX, Cat No. K12-1577) ELISA kits with a modified procedure. The complete procedure was described in Supplementary Document 1. The % inhibition is computed through an equation,

$$\%\ Inhibition = \frac{Abs\ of\ control\ -\ Abs\ of\ sample}{Abs\ of\ control} \times 100$$

Reverse transcriptase inhibitory assay

The reverse transcriptase inhibitory test was carried out according to the manufacturer's procedure (Sigma Aldrich, USA; SKU No. 11468120910). The percentage of reverse transcriptase (RT) inhibition is determined by calculating the ratio of the decrease in RT activity to the control activity, expressed as a percentage,

$$\%\ RT\ inhibition = \frac{Abs\ of\ control\ -\ Abs\ of\ sample}{Abs\ of\ control} \times 100$$

Relative quantification of intracellular HBV DNA and pgRNA by qRT-PCR

The genomic DNA-free nucleic acid (total RNA and viral DNA) was isolated from cells using the RNeasy plus mini kit (Quiagen, Cat No. 74004) according to the manufacturer's instructions. The isolated genomic free nucleic acid was measured using Nanodrop (MAChine). cDNAs were generated using 200ng of genomic-free nucleic acid using the PrimeScript RT Reagent Kit (DSS Takara Bio India, Cat No. RR037A) according to the manufacturer's instructions. The relative expression of HBV pgRNA in each sample was evaluated using real-time qPCR using SYBR green PCR Master Mix (DSS Takara Bio India; Cat No. RR820A) and primers HBVR-F: GAGTGTGGATT CGCACTCC, HBVR-R: GAGGCGAGGGAGTTCTTC T. In addition, the HBV DNA in each sample was measured using particular primers: HBVD-F: GTTGCCCG TTTGTCCTCTAATTC; HBVD-R: GGAGGGATACAT AGAGGTTCCTTGA. RT PCR amplifications were carried out using the BIORAD CFX Maestro (Version 1.1). The cycle conditions were 95 °C for 30 s, followed by 40 cycles of 95 °C for 5 s and 60 °C for 30 s. The mRNA expression was evaluated using the ΔΔCT technique and normalized with respect to beta-actin. The amplification of certain transcripts was further validated by producing dissociation (melting) curve profiles with one cycle from 60 to 95 °C at a 0.5 °C increase for 0.05s [18].

Computational study

Retrieval of phytocompounds and target identification

In continuation of our previous work [17], we prioritized 11 and 3 phytocompounds from AP and TP. The prioritized phytocompounds structures were downloaded from PubChem (https://pubchem.ncbi.nlm.nih.gov/) in SDF format. The conjugate gradients method was used to minimize all of the ligand structures using the "mmff99" forcefield. The gasteigers charges and polar hydrogens were then added, converted the ligand structures into the ".pdbqt" format [19], and subjected to molecular docking studies against the HBx-HBXIP protein complex.

Homology modelling of HBx and HBXIP proteins

Currently, the x-ray crystallographic structure for HBx is not available in the RCSB PDB and hence homology model was used. Due to the absence of sequence homology to any known proteins, HBx received its name "X protein" [20]. The HBx protein was modeled using the RaptorX server (http://raptorx6.uchicago.edu/ContactMap/) [21] and the rank 1 model was retrieved for quality assessments. Further, the HBXIP structure was retrieved from the RCSB PDB (ID: 3MS6; https://www.rcsb.org/structure/3ms6) [22]. The missing amino acids within the structure were filled by the SWISS-MODEL using template-based modelling (https://swissmodel.expasy.org/interactive#structure) [23] and using UniProt accession number O43504 (https://www.uniprot.org/uniprotkb/O43504/entry). The protein structures amino acid distribution was accessed by Ramachandran plot using PROCHECK and the overall quality by ERRAT in SAVES version 6.1 online server (https://saves.mbi.ucla.edu/). The active site of the target was identified using the CASTp server, which utilizes the computed atlas of surface topography of proteins (http://sts.bioe.uic.edu/castp/index.html?1bxw) [24].

Protein-protein docking

Molecular docking of HBx and HBXIP was performed by HADDOCK 2.4 (https://rascar.science.uu.nl/haddock2.4/submit/1) [25] to confirm the interaction of reported amino acids of HBx and HBXIP.

Ligand and protein docking

The ligands were subjected to molecular docking with HBx using AutoDock vina (https://autodock.scripps.edu/) executed through the POAP pipeline [19], and as a result, obtained a total of nine docked conformations for each ligand. The ligand molecule conformation with the lowest binding energy were chosen for visualizing protein-ligand interactions using BIOVIA Discovery Studio Visualizer version 2019.

Molecular dynamics

The structures of the apo form and the protein-ligand complex were subjected to a molecular dynamics (MD) simulation for 100 ns utilizing the Schrodinger Desmond v6.5 program [26] and applying the OPLS force field. The protein structure was positioned in the center of a cuboidal box and solvated using the SPC water model with periodic boundary conditions in all dimensions. The cubic box was positioned at a distance of 10Å from the edges of the protein. The system was neutralized by the addition of Na+/Cl- counter ions. In addition, the SHAKE method was used to constrain the geometry of water molecules, as well as the lengths of bonds and the angles between heavy atoms. The Particle Mesh Ewald approach was used to calculate the long-range interactions between the molecules. The cut-off for Lennard-Jones interactions has been set at 10Å. The system decreased 100.0 ps production run utilizing the OPLS force field. The NPT ensemble was used, using the "Nose-Hoover chain" approach with a relaxation time of 1.0 ps for maintaining the temperature and the "Martyana-Tobias-Klein" method with a relaxation time of 2.0 ps for regulating the pressure. The pressure was maintained at 1.01325 bar and the temperature at 310 K. The Coulombic short-range cut-off radius was determined at 9.0 Å. The complexes were simulated for 100 ns, during which the trajectory was measured at intervals of 10.0 ps. The resulting trajectories were evaluated using the in-built Schrodinger utilities, and the stability parameters were assessed based on our prior work [27–29].

Results

In vitro pharmacology

MTT assay in HepG2.2.15 cell line

The MTT assay showed the CC_{50} of AP (832.915 µg/mL) to be higher than that of the TP (593.122 µg/mL) in HepG2.2.15 at 24 h treatment. Whereas, the CC_{50} of TDF was found to be > 500µM. AP at 2000 and 1000 µg/mL showed about 3.6 and 2.6% cell viability. Whereas, TP showed about 24, and 28% cell viability. This indicates a higher concentration of AP produced significant cytotoxicity. Supplementary Tables 1 and Fig. 2 represent the concentration-dependent percentage of viable cells and CC_{50} value for each test drug.

Time-course analysis of HBsAg and HBeAg

At various time intervals (24, 48, 72, 96, and 120 h), the percentage inhibition of HBsAg secretion in the cell supernatant was calculated. All of the test drugs showed potent HBsAg inhibitory action. AP500 showed about 75% inhibitory effect at 24, 48, and 72 h, and about ~ 95% inhibition was seen at 92 and 120 h. TP500 showed about 70 to 75% inhibition at 24, 48, and 72 h and showed > 80% at 92 and < 80% at 120 h. Whereas, TDF100 showed about 75 to ~ 85% inhibitory effect at 24 h to 120 h. Figure 3 and Supplementary Table 2 represent the HBsAg inhibitory effect of AP, TP, and TDF.

The % inhibition of HBsAg secretion in the cell supernatant was analyzed at different time intervals (24, 48, 72, 96, and 120 h). All the test drugs exhibited strong HBeAg inhibitory activity at 24 h. AP500 showed about 75 to 82% inhibitory effect at 24, 72, and 120 h. TP500, TP250, and TP125 showed about 90% inhibition at 24 h and decreased to > 80% at 72 h and 120 h. Whereas, TDF100 to TDF 6.25 showed about 15 to 25% inhibitory effect at 24 h and no significant inhibitory showed at 72 h and 120 h. Figure 4 and Supplementary Table 3 represent the HBeAg inhibitory effect of AP, TP, and TDF.

HBx-HBP interaction inhibition assay

Figure 5 represents the % HBx-HBXIP interaction inhibition by AP and TP. AP showed about 72% inhibition

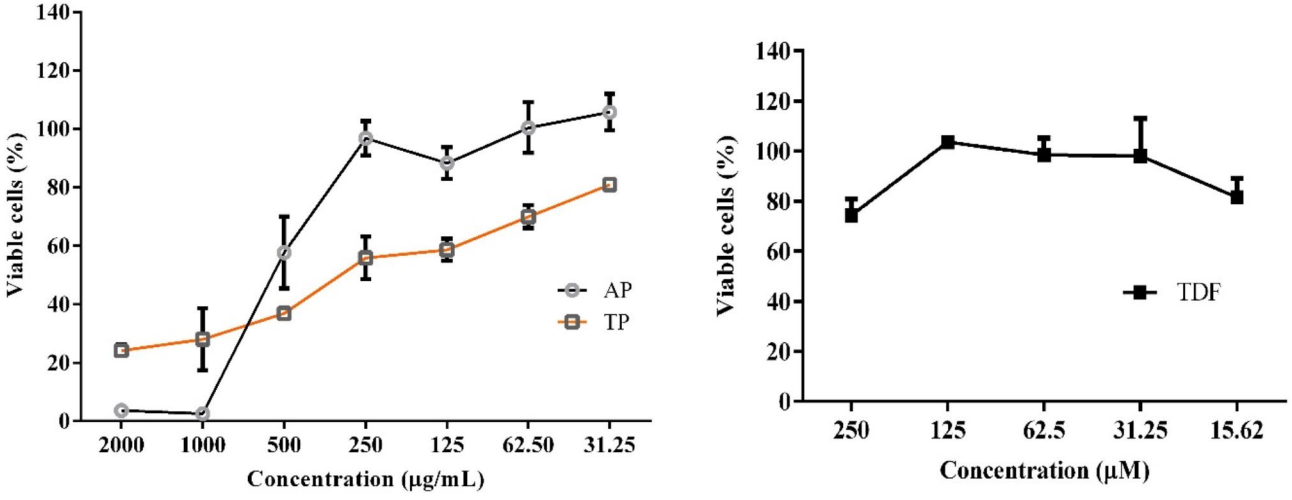

Fig. 2 Concentration-dependent cytotoxicity of AP, TP, and TDF in HepG2.2.15 cell line

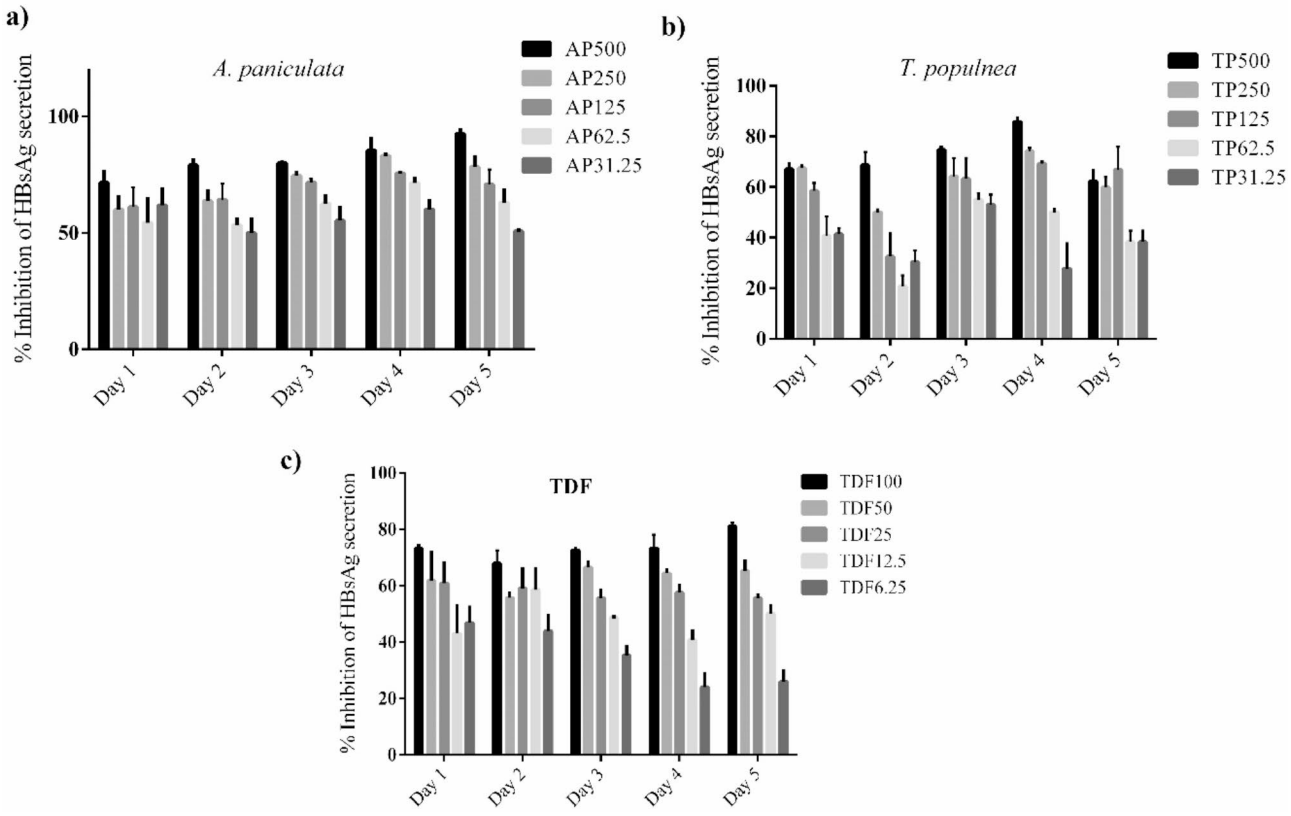

Fig. 3 Time and concentration-dependent HBsAg secretion inhibition of AP, TP, and TDF

at 500 µg/mL and about 57% inhibition at 62.5 µg/mL. The IC_{50} of AP was found to be < 62.5 µg/mL for HBx-HBXIP interaction inhibition. TP showed about 31.48% inhibition at 500 µg/mL. The IC_{50} of TP was found to be 806.69 µg/mL.

Reverse transcriptase inhibitory assay

AP and TP showed dose-dependent RT inhibition (Fig. 6). The IC_{50} of AP and TP was found to be 304.52 µg/mL and 553.88 µg/ml, respectively. Whereas, TDF did not exhibit RT inhibitory action at a concentration of 250µM (IC_{50} > 250 µM).

Relative quantification of intracellular HBV DNA and pgRNA by qRT-PCR

As Fig. 7 shows, treatment of HepG2.2.15 cells with AP 125, 250, and 500 µg/mL for 24 h decreased the intracellular HBV DNA by 2^5 fold. Whereas, AP 62.5 and 31.25 µg/mL decreased by 2^4 and 2^3 fold respectively. Similarly, AP 125, 250, and 500 µg/mL showed 2^1 fold decrease in pgRNA level. TP 500 µg/mL showed 2^6 fold decreases in intracellular HBV DNA and TP 250, 125, 62.5 µg/mL showed 2^4 fold decreases in intracellular HBV DNA. TP didn't show any significant effect on pgRNA level. Whereas, the TDF concentration range between 6.25 to 100µM didn't show a significant effect on intracellular HBV DNA and pgRNA levels. TDF 100, 50, and 25 µM showed about 2^2 fold decrease in intracellular HBV DNA.

Computational pharmacology

Homology modelling of HBx and HBXIP proteins

The homology model of HBx and HBXIP was generated using the Raptorx and SWISS-MODEL servers, respectively, and validated for its overall quality by the ERRAT server which was 78.76% and 92.5%. Further, the stereochemical properties were analyzed using the Ramachandran plot. In the HBx protein, 72.4% residues in the most favoured, 19.7% in the additionally allowed region, 4.7% in the generously allowed region, and 3.1% in the disallowed region. Likewise, in the HBXIP protein, 84.8% and 15.2% residues in the most favoured and additionally allowed region, respectively. No residues were in the generously and disallowed region. The active site residues of HBx protein are Leu9, Asp14, Val15, Leu16, Arg56, Leu71, Arg72, Tyr73, Thr74, Ser75, Ala76, Arg78, Glu80, and Lys95 and the active site residues of HBXIP are Supplementary Fig. S1 and S2 shows the HBx and HBXIP protein (a) Ramachandran plot and (b) overall quality respectively.

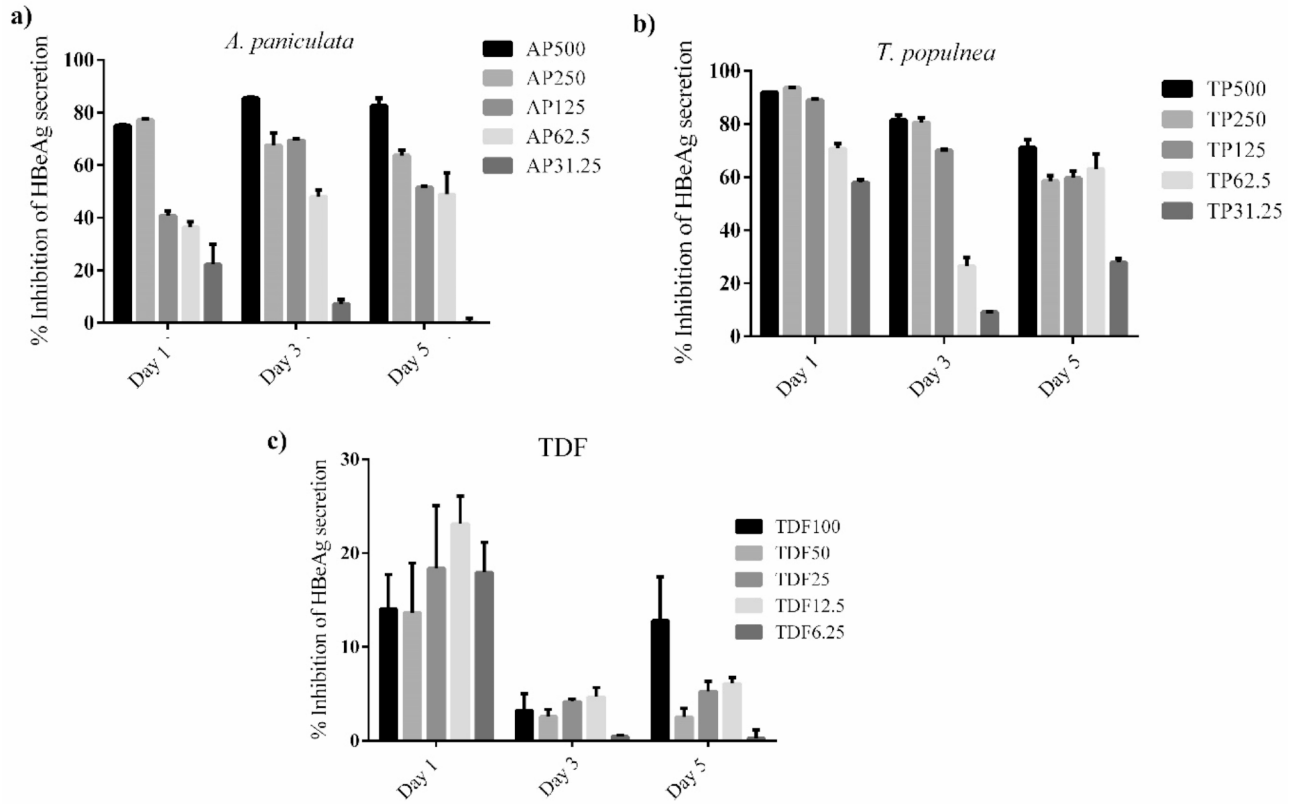

Fig. 4 Time and concentration-dependent HBeAg secretion inhibition of AP, TP, and TDF

Protein-protein docking

The HBx-HBXIP protein complex showed the least BE of -172.385 in the haddock server. Thr36, Asp70, Glu40, Asn71 of HBXIP was found to interact with Lys140, Lys130, Arg4, His139 of HBx with a distance of 2.76Å, 2.66Å, 2.69Å, 3.02Å respectively (Fig. 8). Previously, it is reported that residues 137CRHK140 within HBx are necessary for binding T36 HBXIP [22].

Ligand-protein docking

Similarly, 11 compounds from *A. paniculata* and 3 from *T. populnea* were virtually screened against HBx protein. Among them, Kaempferol-7-Glucoside from *T. populnea* showed the least BE of -6.6 kcal/mol with HBx via forming four hydrogen bonds interaction with Lys130, Val133 (2), Trp120 and two hydrophobic bonds with Phe132 and Ile127. Andrographidine C from *A. paniculata* was found to be the best lead hit against HBx as it formed two hydrogen bonds with Val131, and Thr91 and four hydrophobic interactions with Ala85, Val133 (2), and His139. Among these residues, His139 was identified to interact with HBXIP. Similarly, 5-Hydroxy-7,8,2',3'-Tetramethoxyflavone, 5-Hydroxy-2',3',4',7,8-Pentamethoxyflavone, 5-Hydroxy-7,8-Dimethoxyflavone, 5-Hydroxy-7,8,2'-Trimethoxyflavone, and 5,4'-Dihidroxy-7,8,2',3'-Tetramethoxyflavone were also found to be the next best lead hits against HBx as these compounds scored least BE range of -6.0 to -5.7 kcal/mol and formed interaction with Cys137. This residue is reported to interact with HBXIP. Compounds from *T. populnea* i.e. Kaempferol-7-Glucoside, Herbacetin, and Gossypetin didn't form interaction with 137CRHK140 of HBx. Table 1 represents the intermolecular interaction of compounds with HBx and Fig. 9 represents the interaction of Andrographidine C with HBx.

Molecular dynamics

Stability of HBx-HBXIP protein complex

The HBx-HBXIP complex exhibited stable dynamics throughout the 100 ns simulation. The average backbone RMSD was found to be ~6.5 Å. The RMSF plot revealed that Cys137, Arg138, His139, and Lys140 which are essential to interact with HBXIP showed lesser fluctuation (~3.0 Å). Whereas, the loop region showed larger fluctuations up to 7 Å. Figure 10 represents the binding mode and stability interaction fraction of HBx with HBXIP with 20ns time interval up to 100 ns.

Stability of andrographidine C with HBx

The Andrographidine C with HBx showed stable dynamics during the 100ns of simulation (Fig. 11). The average backbone and complex RMSDs for Andrographidine C were 6.58 Å and ~6.24 Å, respectively. Initially, a steady

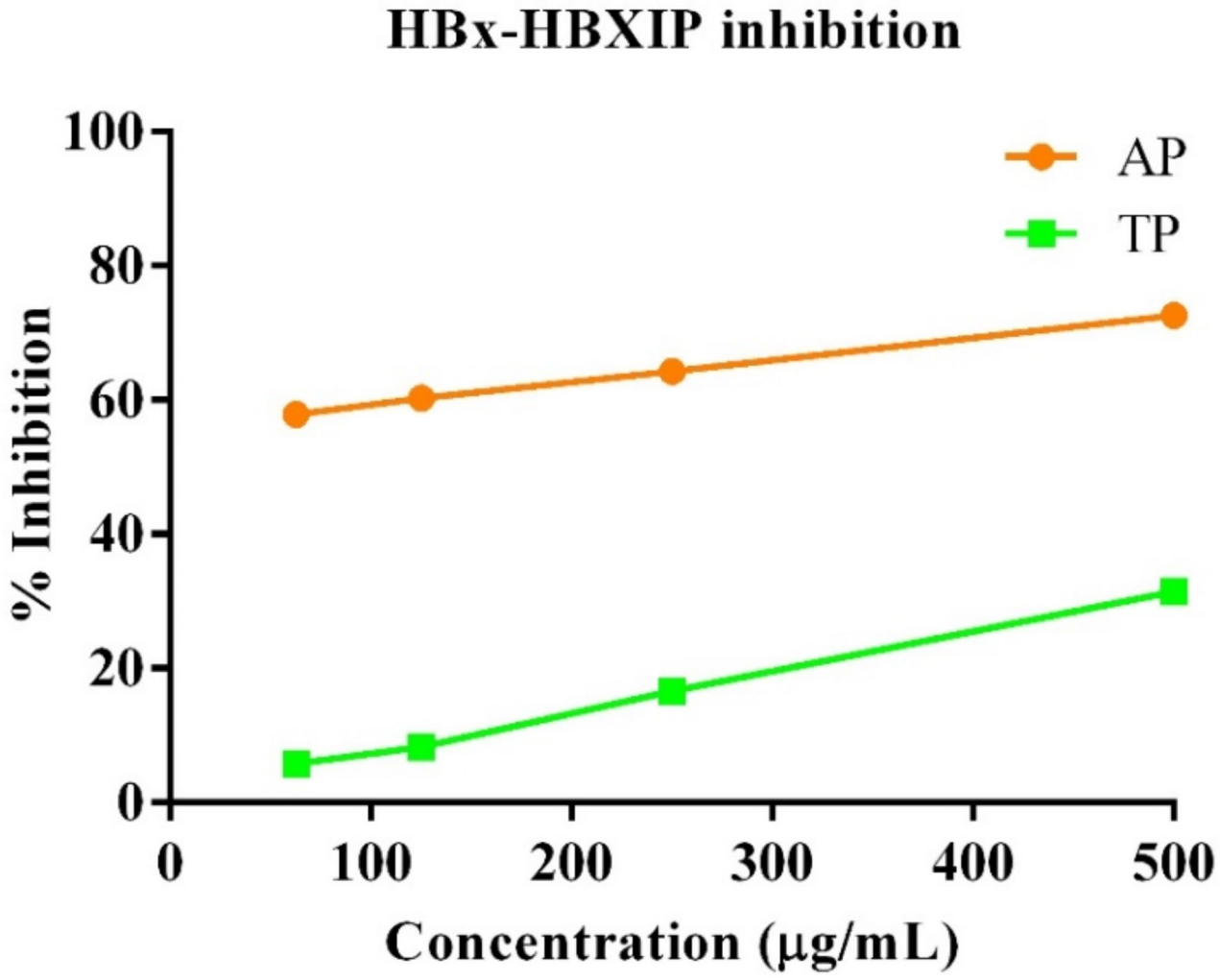

Fig. 5 Concentration-dependent HBx-HBXIP interaction inhibition and IC_{50} of AP and TP

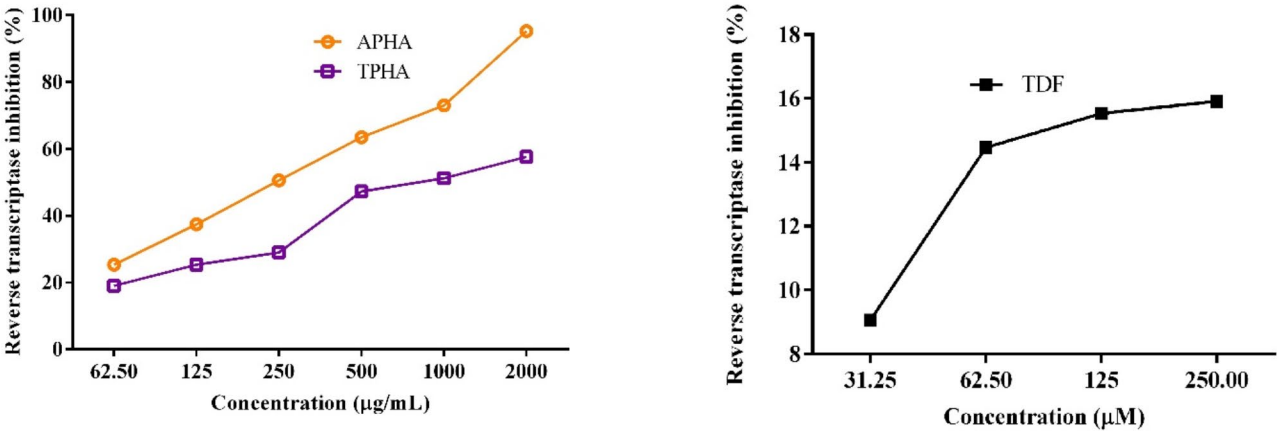

Fig. 6 Concentration-dependent RT inhibitory activity of AP and TP

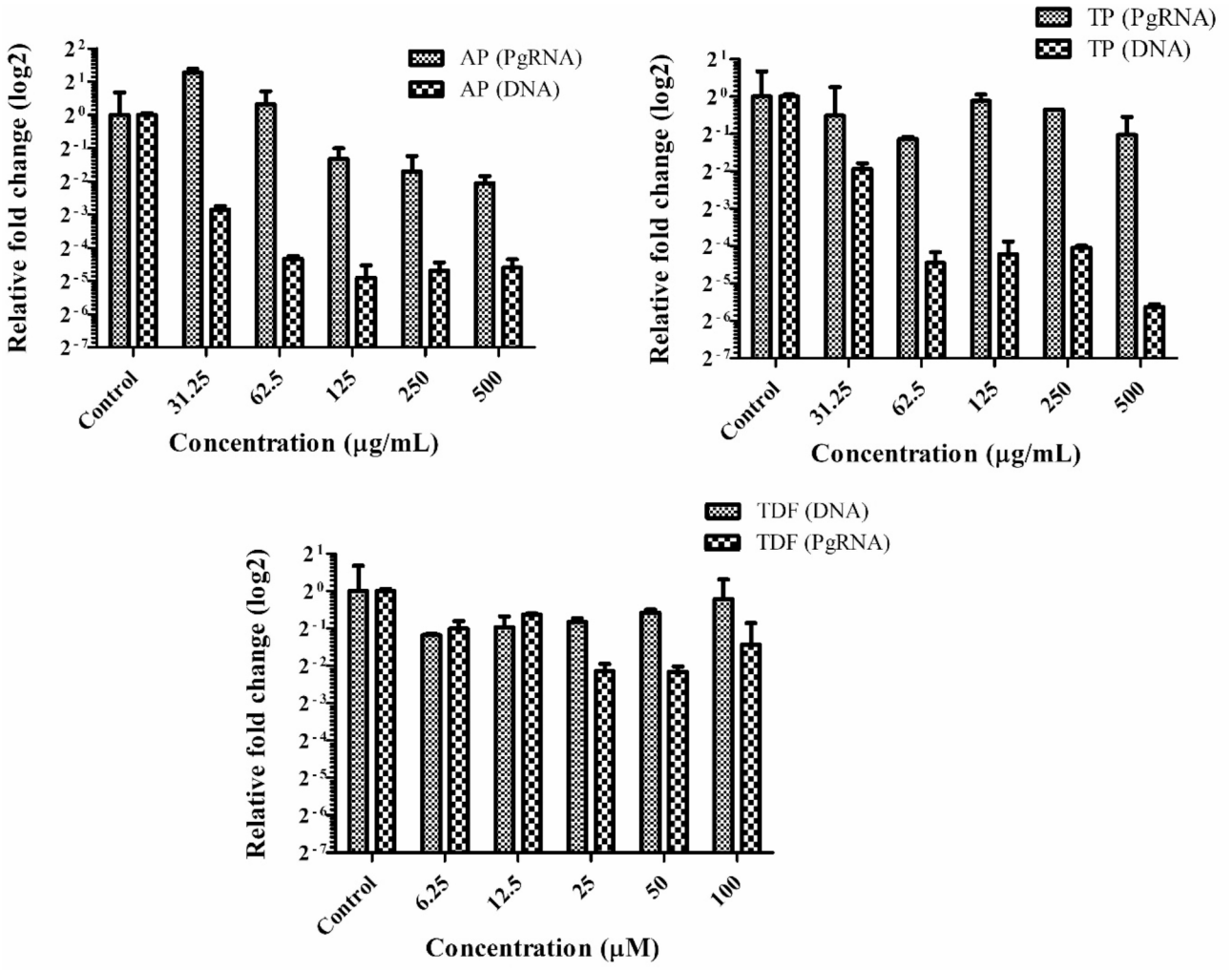

Fig. 7 Effect of AP, TP, and TDF on intracellular HBV DNA and pgRNA in HepG2.2.15 cell line by qRT-PCR

decrease in the complex RMSD was observed from 0 to 25 ns, and a fluctuation was observed from 25 ns to 63 ns, further stabilized throughout 100 ns simulation. This was due to the opening and closure of the binding pocket from 25 to 63ns and 63ns to 100ns respectively which is evidenced by a gradual increase in the Rg value (~16.5 Å to ~19ns) at 20 to 63ns and a steady decrease in the Rg value from 63ns to 100ns. The RMSF plot revealed that the residues engaged in the stable and conserved non-bonded interactions mainly Arg138, His139, and Lys140 showed relatively smaller fluctuations (~3 Å). However, the loop regions showed higher residual fluctuation up to 12 Å. The Andrographidine C with HBx interaction plot revealed that Andrographidine C had better contact with Arg138 and His139 from 0 to 50 ns and with Lys140, and Trp141 from 50 to 82 ns. The interaction fraction diagram revealed that Andrographidine C formed 7% interaction with Arg138, 5% with His139, and 12% with Lys140 throughout the simulation.

Discussion

The present study elucidated the anti-HBV potential of two important medicinal plants AP and TP using in vitro studies combined with multiple bioinformatics approaches. Currently, the progress in developing medicines to combat HBV has been hindered by the dearth of appropriate experimental models capable of precisely imitating normal chronic hepatitis B [30]. In our previous study [17], phytocompounds of AP and TP were identified as modulators of genes involved HBV induced HCC *via* network pharmacology analysis, and this study was further extended to validate them as an anti-HBV agent through in vitro studies, molecular docking, and dynamics. Initially, the effect of hydroalcoholic extract of AP and TP was tested for cytotoxicity in HepG2.2.15 cells. Further, tested for HBsAg (a serological marker for viral infection) and HBeAg level (a serological marker for active DNA replication), RT inhibition via measuring the intracellular DNA and pgRNA level, and HBx-HBXIP interaction inhibition capacity in using HepG2.2.15 cell

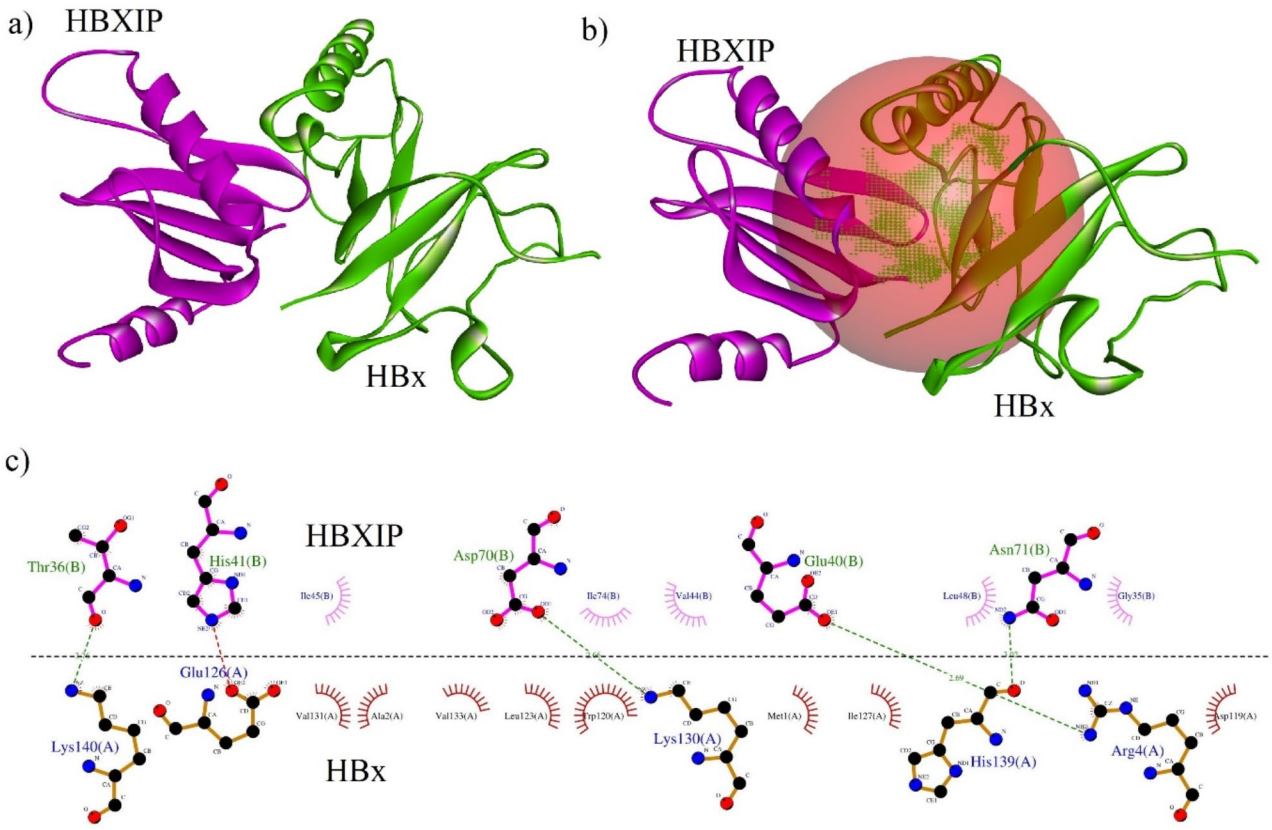

Fig. 8 Binding mode of HBx with HBXIP. (**a**) HBx-HBXIP, (**b**) HBx-HBXIP binding pocket, and (**c**) Interactions between HBx and HBXIP

line and the reported phytocompounds from AP and TP mode of action on HBx protein was further inferred using molecular modelling techniques viz., protein-protein and protein-ligand docking and molecular dynamics simulation studies.

Firstly, the MTT assay results demonstrated significant insights into the cytotoxic effects of AP, TP, and TDF on the HepG2.2.15 cell line. The CC_{50} values, which denote the concentration required to kill 50% of the cell population, were found to be 832.915 µg/mL for AP and 593.122 µg/mL for TP at 24 h. These values indicate that AP is less cytotoxic compared to TP. In contrast, TDF exhibited a CC_{50} value greater than 500µM, suggesting a lower cytotoxicity at the tested concentrations. When analyzing cell viability at higher concentrations, AP exhibited cytotoxicity, with cell viability at about 3.6% and 2.6% at 2000 and 1000 µg/mL, respectively. TP showed slightly higher cell viability at these concentrations, with 24% and 28% viability, respectively. This suggests the potent cytotoxic nature of AP at higher doses, which could be leveraged in therapeutic contexts where high cytotoxicity towards infected cells is desired.

Further, the time-course analysis of HBsAg and HBeAg secretion in the serum was analyzed and it provides critical insights into the antiviral efficacy of the tested compounds. AP at 500 µg/mL exhibited a robust inhibitory effect on HBsAg, with approximately 75% inhibition observed at 24, 48, and 72 h, escalating to about 95% at 92 and 120 h. Similarly, TP at 500 µg/mL showed 70–75% inhibition initially, rising to over 80% at 92 h, but slightly decreasing at 12 h. TDF maintained a consistent inhibition rate between 75% and 85% throughout the 24 to 120 h period. The HBeAg inhibition profile further highlights the potential of AP and TP. AP at 500 µg/mL achieved 75–82% inhibition, whereas TP, even at lower concentrations (125 µg/mL), displayed around 90% inhibition at 24 h, although this reduced to above 80% at 72 and 120 h. TDF, however, exhibited limited efficacy against HBeAg, with only 15–25% inhibition observed at 24 h, and no significant inhibition was observed. This suggests that while TDF is effective against HBsAg, its impact on HBeAg is minimal, indicating a potential advantage for AP and TP in comprehensive antiviral strategies.

The HBx plays a crucial role in the viral life cycle which exhibits a diverse array of biological functions, and has shown great potential in influencing the onset and progression of virus-associated HCC via modulating transcription and transactivation processes. The processes of this process entail the regulation of gene transcription,

Table 1 Intermolecular interaction of phytocompounds with HBx protein

Plant name	Compound name	PubChem ID	BE (kcal/mol)	HBI	NHBI	Interaction with active site (Yes/No)
Thespesia populnea	Kaempferol-7-Glucoside	10,095,180	-6.6	Lys130, Val133 (2), Trp120	Phe132, Ile127 (2), Glu121	No
Andrographis paniculata	Andrographidine C	5,318,484	-6.4	Val131, Thr91	Ala85, Val133 (2), His139	Yes
Thespesia populnea	Gossypetin	5,280,647	-6.3	Nil	Phe132,Val133	No
Andrographis paniculata	Wightin	12,444,943	-6.1	Nil	Val133, Phe132	No
Andrographis paniculata	2'-Hydroxy-5,7,8-Trimethoxyflavone	21,668,878	-6.1	Val133, Lys130	Phe132, Ile127, Val131, Glu121	No
Andrographis paniculata	5-Hydroxy-7,8,2',3'-Tetramethoxyflavone	141,423,924	-6	Tyr111, Lys130	Phe132, Lys130, Val133 (2), Cys137	Yes
Andrographis paniculata	5-Hydroxy-2',3',4',7,8-Pentamethoxyflavone	12,315,479	-6	Tyr111, Lys130 (2)	Phe132, Val133, Cys137	Yes
Andrographis paniculata	5-Hydroxy-7,8-Dimethoxyflavone	188,316	-6	Val133	Phe132, Val133 (2), Cys137	Yes
Andrographis paniculata	Skullcapflavone I	5,320,399	-5.9	Val131	Phe132, Val133	No
Thespesia populnea	Herbacetin	5,280,544	-5.9	Glu121, Lys140	Phe132, Ile127 (2)	No
Andrographis paniculata	5-Hydroxy-7,8,2'-Trimethoxyflavone	44,258,542	-5.8	Val133	Val133 (2), Cys137, Phe132	Yes
Andrographis paniculata	5-Hydroxy-7,8,2',5'Tetramethoxyflavone	10,948,318	-5.7	Lys130, Trp120	Ile127 (2), Phe132, Glu121, Glu126	No
Andrographis paniculata	5,4'-Dihidroxy-7,8,2',3'-Tetramethoxyflavone	13,963,777	-5.7	Lys130	Val133, Cys137	Yes
Andrographis paniculata	Altisin	15,100,719	-5.3	Val133, Lys130, Tyr111	Phe132 (3), Ala85, Arg87	No

BE, Binding Energy; HBI, Hydrogen Bond Interaction; NHBI, Non-Hydrogen Bond Interaction

cell signal transduction, cell proliferation and transformation, cell cycle, and cell apoptosis [31], making it a critical target for therapeutic intervention. Its interaction with HBXIP, a cellular protein, is essential for various HBx-mediated effects, including transcriptional regulation and cellular proliferation. Therefore, inhibiting this interaction is a promising strategy for therapeutic intervention. The development of the HBx-HBxIP interaction inhibition assay represents a significant advancement in this study. By using a modified protocol, we performed the HBx-HBxIP interaction inhibition assay. In this study, the HBx-HBXIP interaction inhibition assay results show that AP significantly disrupts this interaction, showing about 72% inhibition at 500 µg/mL and 57% at 62.5 µg/mL, with an IC_{50} of less than 62.5 µg/mL. TP, in comparison, showed only 31.48% inhibition at 500 µg/mL and an IC_{50} of 806.69 µg/mL, indicating a lower efficacy. These results suggest the potent inhibitory action of AP on the HBx-HBXIP interaction, positioning it as a superior candidate for targeting this critical protein-protein interaction.

The quantitative analysis of intracellular HBV DNA and pgRNA via qRT-PCR provides a deeper understanding of the antiviral mechanisms. AP at concentrations of 125, 250, and 500 µg/mL reduced HBV DNA by 2^5-fold, while lower concentrations (62.5 and 31.25 µg/mL) showed about 2^3-2^4 fold reductions. Similarly, no significant effect of AP on pgRNA levels, even at higher concentrations showed about 2^1-fold decrease in the pgRNA. TP also demonstrated a profound impact on HBV DNA, with up to 2^6-fold reduction at 500 µg/mL, but did not significantly affect pgRNA levels. TDF, while effective at reducing HBV DNA (2^2-fold decrease at 100 µM) showed negligible impact on pgRNA. This differential effect on pgRNA by AP and TP versus TDF suggests distinct mechanisms of action, where AP appears to interfere more comprehensively with viral replication processes. The ability of AP to reduce both HBV DNA and pgRNA levels highlights its potential as a robust antiviral agent. Previous in vivo studies using hepatitis B transgenic mice have provided valuable insights into the effects of andrographolide on HBV and reported a decrease in HBV DNA levels and an improvement in liver histopathology, supporting the therapeutic potential. Dehydroandrographolide and andrographolide from AP showed inhibitory effects on HBV DNA replication in HepG2.2.15 cells with IC_{50} values of 22.58 and 54.07 µM, respectively [32].

The computational analyses involving homology modeling, protein-protein docking, protein-ligand docking, and molecular dynamics simulation provide valuable insights into the molecular interactions and stability of the compounds with protein targets. The homology models for HBx and HBXIP proteins were carried

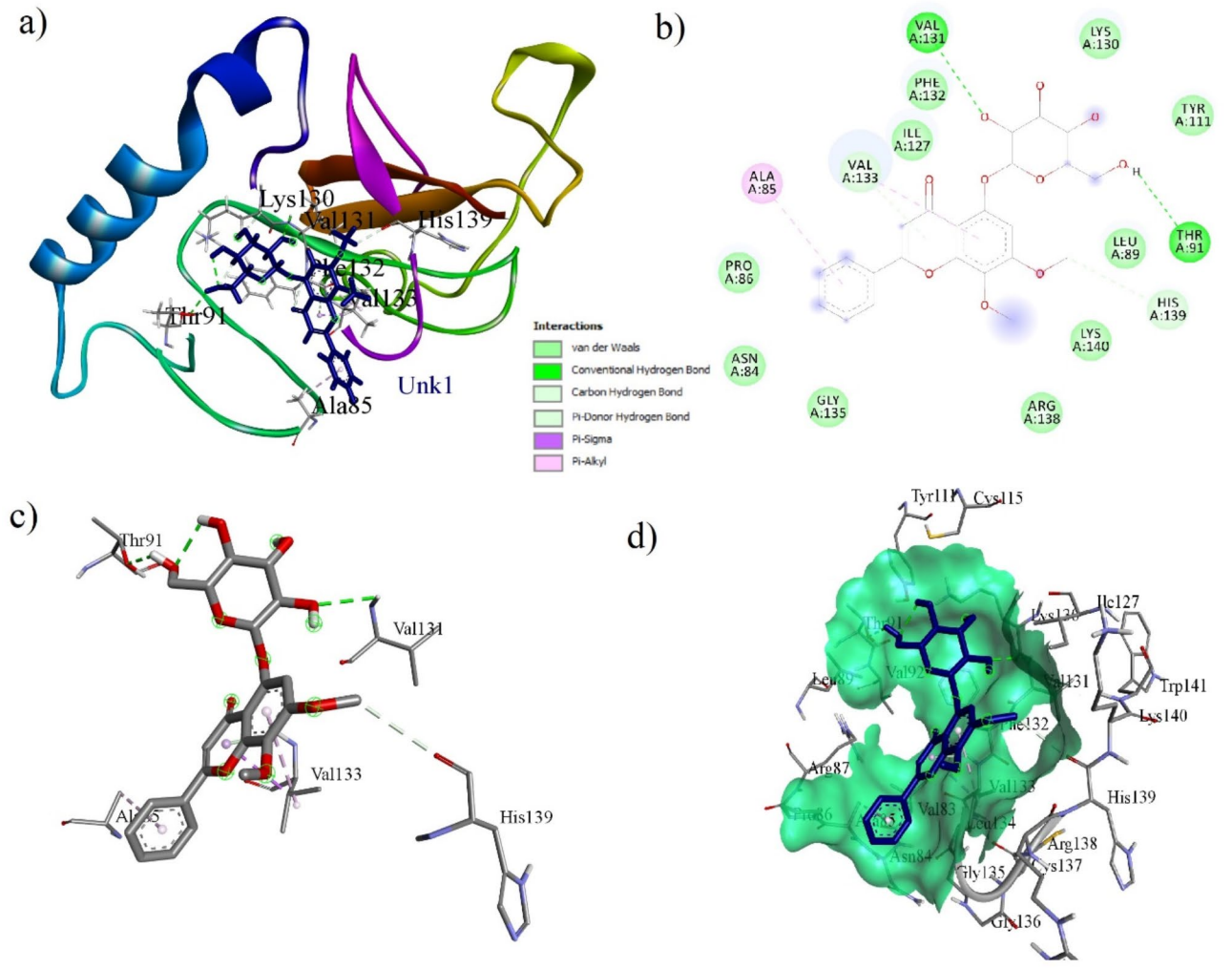

Fig. 9 Intermolecular interaction of Andrographidin C with HBx. (**a**) protein-ligand complex, (**b**) 2D interactions picture, (**c**) 3D representation, and (**d**) pocket representation of Andrographidin C with HBx

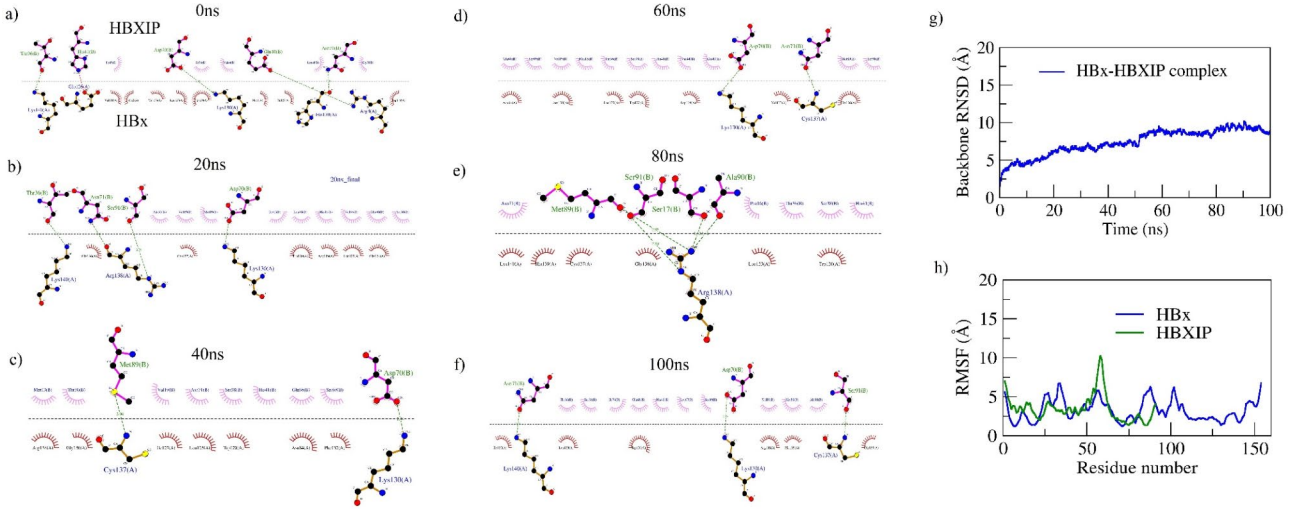

Fig. 10 Stability interaction fraction of HBx with HBXIP during 100ns MD run with 20ns interval frame analysis. (**a**) 0ns frame, (**b**) 20ns frame, (**c**) 40ns frame, (**d**) 60ns frame, (**e**) 80ns frame, (**f**) 100ns frame, (**g**) RMSD of HBx-HBXIP complex during 100ns, and (h) RMSF of C-alpha atoms of HBx and HBXIP

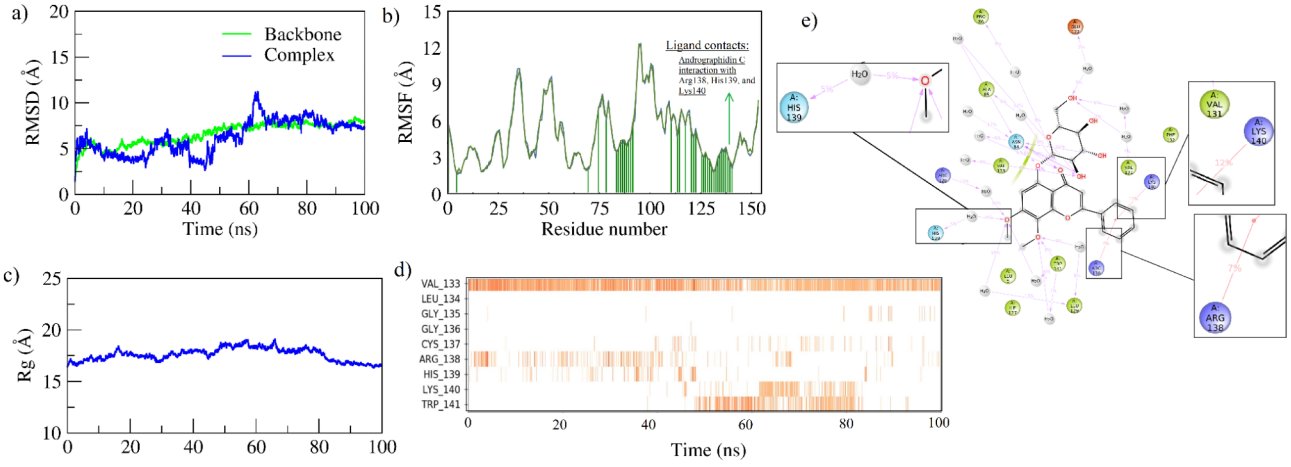

Fig. 11 Stability of Andrographin C with HBx during 100ns MD run. (**a**) Backbone and complex atoms RMSD, (**b**) RMSF with residue-wise ligand contacts (shown in vertical green line), (**c**) Rg of HBx, (**d**) and (**e**) Interaction fraction between Andrographin C and HBx throughout 100ns

out and validated for quality and their residues in the favourable region in the Ramachandran plot. Further, the protein-protein docking results indicated strong interactions between HBx and HBXIP, with key residues Lys140, Lys130, Arg4, and His139 playing crucial roles. Notably, these residues also showed significant interactions with lead compounds from AP and TP, particularly Andrographidine C from AP. Molecular dynamics simulations further validated the stability of the HBx-HBXIP complex and the interactions of Andrographidine C with HBx. The HBx-HBXIP complex remained stable throughout the 100 ns simulation, with essential residues showing minimal fluctuations. The dynamic behavior of Andrographidine C, characterized by stable RMSD values and consistent interactions with key residues (Arg138, His139, and Lys140), highlights its potential as a potent inhibitor. The simulations revealed that the binding pocket of HBx underwent conformational changes, which were well-accommodated by Andrographidine C, maintaining strong interactions throughout the simulation. This stable binding of Andrographidine C to HBx suggests its efficacy in disrupting HBx functions, further supporting its candidacy as a therapeutic agent.

Conclusion

The comprehensive analysis of AP, TP, and TDF in the HepG2.2.15 cell line reveals distinct advantages and potential therapeutic applications in treating HBV infection. AP, with its lower CC_{50} and significant inhibitory effects on HBsAg, HBeAg, HBx-HBXIP interaction, and HBV DNA and pgRNA levels, emerges as a highly effective antiviral agent. TP, while also effective, shows slightly lower efficacy in certain assays but still presents a valuable alternative, particularly given its strong inhibition of HBeAg and HBV DNA. The computational and molecular dynamics studies provide robust support for the experimental findings, showcasing the potential of specific compounds, particularly flavonoids like Andrographidine C, in targeting critical viral interactions. These insights pave the way for further screening of AP and TP-derived compounds as potent antiviral agents against HBV. Future research should focus on in vivo studies and clinical trials to validate these findings and explore the full therapeutic potential of these natural compounds. Additionally, exploring combination therapies with AP, TP, and conventional antiviral drugs like TDF could yield synergistic effects, enhancing overall treatment efficacy and reducing the risk of resistance development.

Supplementary Information

The online version contains supplementary material available at https://doi.org/10.1186/s12906-025-04807-z.

Supplementary Material 1

Supplementary Material 2

Supplementary Material 3

Acknowledgements

The authors gratefully acknowledge the extramural funding of the Indian Council of Medical Research, Department of Health Research, New Delhi (ICMR grant No. ISRM/12(61)2019) and the intramural funding of the ICMR-National Institute of Traditional Medicine, Belagavi for providing resources. Vishal S. Patil is thankful to the KLE Academy of Higher Education and Research, Belagavi, India, for supporting his Ph.D. studies.

Author contributions

Author Contributions: VSP: Methodology, Validation, Formal analysis, Investigation, Data curation, and Writing—original draft; DRH: Conceptualization, Resources, Writing—original draft, Writing—review and editing, Validation, Supervision, Project administration, and Funding acquisition; RC, VVB, SSG, FAB, PPP: Writing—review and editing; SSJ, SR: Formal analysis, Supervision and Writing—review and editing, HVH: Resources, Writing—review and editing. All authors reviewed the manuscript.

Funding
This study was funded by the Indian Council of Medical Research, Department of Health Research, New Delhi (ICMR grant no. ISRM/12(61)2019) and ICMR-National Institute of Traditional Medicine, Belagavi, India.

Data availability
The authors confirm that the data supporting the findings of this study are available within the article and/or its Supplementary Materials. Information on 14 compounds (11 from ***Andrographis paniculata*** and 3 from ***Thespesia populnea***) as modulators of hepatocellular carcinoma induced by HBV, can be found in our previously published article [reference number 17]. Additional data will be provided upon request to the corresponding authors.

Declarations

Ethics approval and consent to participate
Permission for the collection of *Andrographis paniculata* and *Thespesia populnea* was not applicable. Approval was obtained from the Institutional Biosafety Committee (IBSC), RCGM-DBT, Government of India, for conducting research on the HepG2.2.15 cell line for anti-HBV activity (Letter No: BT/IBKP/475/2021; IBKP TAI No: C100753).

Consent for publication
Not applicable.

Institutional review board statement
Not applicable.

Informed consent statement
Not applicable.

Competing interests
The authors declare no competing interests.

Author details
[1]ICMR-National Institute of Traditional Medicine, Nehru Nagar, Belagavi, Karnataka 590010, India
[2]KLE College of Pharmacy, Belagavi, KLE Academy of Higher Education and Research, Nehru Nagar, Belagavi,, Karnataka 590010, India

Received: 14 July 2024 / Accepted: 3 February 2025
Published online: 08 March 2025

References

1. Glebe D, Bremer CM. The molecular virology of hepatitis B virus. Semin Liver Dis. 2013;33(2):103–12.
2. Bianca C, Sidhartha E, Tiribelli C, El-Khobar KE, Sukowati CH. Role of hepatitis B virus in development of hepatocellular carcinoma: focus on covalently closed circular DNA. World J Hepatol. 2022;14(5):866.
3. Marchetti AL, Guo H. New insights on molecular mechanism of hepatitis B virus covalently closed circular DNA formation. Cells. 2020;9(11):2430.
4. Tsukuda S, Watashi K. Hepatitis B virus biology and life cycle. Antiviral Res. 2020;182:104925.
5. World Health Organization, Hepatitis B. May. Available from: https://www.who.int/news-room/fact-sheets/detail/hepatitis-b. Accessed on 22 2024.
6. Easterbrook PJ, Luhmann N, Bajis S, Min MS, Newman M, Lesi O, Doherty MC. WHO 2024 hepatitis B guidelines: an opportunity to transform care. Lancet Gastroenterol Hepatol. 2024;9(6):493–5.
7. Li Y, Zhou J, Li T. Regulation of the HBV entry receptor NTCP and its potential in hepatitis B treatment. Front Mol Biosci. 2022;9:879817.
8. van Hemert FJ, van de Klundert MA, Lukashov VV, Kootstra NA, Berkhout B, Zaaijer HL. Protein X of hepatitis B virus: origin and structure similarity with the central domain of DNA glycosylase. PLoS ONE. 2011;6(8).
9. Sivasudhan E, Blake N, Lu Z, Meng J, Rong R. Hepatitis B viral protein HBx and the molecular mechanisms modulating the hallmarks of hepatocellular carcinoma: a comprehensive review. Cells. 2022;11(4):741.
10. Wong GH, Seto WK, Wong VS, Yuen MF, Chan HY. Long-term safety of oral anti-viral treatment for chronic hepatitis B. Aliment Pharmacol Ther. 2018;47(6):730–7.
11. Clark DN, Hu J. Hepatitis B virus reverse transcriptase–target of current antiviral therapy and future drug development. Antiviral Res. 2015;123:132–7.
12. Hadziyannis SJ, Tassopoulos NC, Heathcote EJ, Chang TT, Kitis G, Rizzetto M, Marcellin P, Lim SG, Goodman Z, Ma J, Arterburn S. Long-term therapy with adefovir dipivoxil for HBeAg-negative chronic hepatitis B. N Engl J Med. 2005;352(26):2673–81.
13. Hadziyannis SJ, Tassopoulos NC, Heathcote EJ, Chang TT, Kitis G, Rizzetto M, Marcellin P, Lim SG, Goodman Z, Ma J, Brosgart CL. Long-term therapy with adefovir dipivoxil for HBeAg-negative chronic hepatitis B for up to 5 years. Gastroenterology. 2006;131(6):1743–51.
14. Lok AS, Lai CL, Leung N, Yao GB, Cui ZY, Schiff ER, Dienstag JL, Heathcote EJ, Little NR, Griffiths DA, Gardner SD. Long-term safety of lamivudine treatment in patients with chronic hepatitis B. Gastroenterology. 2003;125(6):1714–22.
15. Lai CL, Gane E, Liaw YF, Hsu CW, Thongsawat S, Wang Y, Chen Y, Heathcote EJ, Rasenack J, Bzowej N, Naoumov NV. Telbivudine versus lamivudine in patients with chronic hepatitis B. N Engl J Med. 2007;357(25):2576–88.
16. Hong M, Li S, Tan HY, Wang N, Tsao SW, Feng Y. Current status of herbal medicines in chronic liver disease therapy: the biological effects, molecular targets and future prospects. Int J Mol Sci. 2015;16(12):28705–45.
17. Patil VS, Harish DR, Vetrivel U, Deshpande SH, Khanal P, Hegde HV, Roy S, Jalalpure SS. Pharmacoinformatics analysis reveals flavonoids and diterpenoids from Andrographis paniculata and Thespesia populnea to target hepatocellular carcinoma induced by hepatitis B virus. Appl Sci. 2022;12(21):10691.
18. Patil VS, Harish DR, Charla R, Vetrivel U, Jalalpure SS, Bhandare VV, Deshpande SH, Hegde HV, Roy S. Structural insights into modeling of hepatitis B virus reverse transcriptase and identification of its inhibitors from potential medicinal plants of Western ghats: an in silico and in vitro study. J Biomol Struct Dyn. 2024;42;11731–49.
19. Samdani A, Vetrivel U. POAP: a GNU parallel based multithreaded pipeline of open babel and AutoDock suite for boosted high throughput virtual screening. Comput Biol Chem. 2018;74:39–48.
20. Murakami S. Hepatitis B virus X protein: structure, function and biology. Intervirology. 1999;42(2–3):81–99.
21. Källberg M, Margaryan G, Wang S, Ma J, Xu J. RaptorX server: a resource for template-based protein structure modeling. Protein Struct Prediction. 2014;1137:17–27.
22. Garcia-Saez I, Lacroix FB, Blot D, Gabel F, Skoufias DA. Structural characterization of HBXIP: the protein that interacts with the anti-apoptotic protein survivin and the oncogenic viral protein HBx. J Mol Biol. 2010;405(2):331–40.
23. Schwede T, Kopp J, Guex N, Peitsch MC. SWISS-MODEL: an automated protein homology-modeling server. Nucleic Acids Res. 2003;31(13):3381–5.
24. Tian W, Chen C, Lei X, Zhao J, Liang J. CASTp 3.0: computed atlas of surface topography of proteins. Nucleic Acids Res. 2018;46:W1.
25. Dominguez C, Boelens R, Bonvin AM. HADDOCK: a protein– protein docking approach based on biochemical or biophysical information. J Am Chem Soc. 2003;125(7):1731–7.
26. Bowers KJ, Chow E, Xu H, Dror RO, Eastwood MP, Gregersen BA, Klepeis JL, Kolossvary I, Moraes MA, Sacerdoti FD, Salmon JK, Shan Y, Shaw DE. Scalable algorithms for molecular dynamics simulations on commodity clusters. Proceedings of the ACM/IEEE Conference on Supercomputing (SC06), Tampa, Florida, 2006, November 11–17.
27. Bhattacharya K, Khanal P, Patil VS, Dwivedi PS, Chanu NR, Chaudhary RK, Deka S, Chakraborty A. Computational pharmacology profiling of borapetoside C against melanoma. J Biomol Struct Dyn. 2024;42(6):3233–48.
28. Patil VS, Dodakallanavar J, Khanal P, Patil BM, Chaudhary RK, Shrivastava AK, Chanu NR, Harish DR, Mateti UV. Computational modelling of BACE-1, AChE, and phosphodiesterase inhibitors as anti-alzheimer's agents. In: Bhattacharya K, Bhattacharjee A, editors. Computational and Experimental Studies in Alzheimer's Disease. CRC Press; 2024. pp. 122–37.
29. Galagali A, Patil VS, Hiremath K, Sampat GH, Patil R, Virge R, Harish DR, Hedge HV, Roy S. Investigation of alpha amylase inhibitors from Bidens pilosa L. by in silico and in vitro studies. Silico Pharmacol. 2024;12(1):9.
30. Liu Y, Maya S, Ploss A. Animal models of hepatitis B virus infection–success, challenges, and future directions. Viruses. 2021;13(5):777.
31. Xu Q, Gu S, Liang J, Lin Z, Zheng S, Yan J. The biological function of hepatitis B virus X protein in hepatocellular carcinoma. Oncol Res. 2019;27(4):509.

32. Chen H, Ma YB, Huang XY, Geng CA, Zhao Y, Wang LJ, Guo RH, Liang WJ, Zhang XM, Chen JJ. Synthesis, structure–activity relationships and biological evaluation of dehydroandrographolide and andrographolide derivatives as novel anti-hepatitis B virus agents. Bioorg Med Chem Lett. 2014;24(10):2353–9.